Nanoscale

PAPER

View Article Online
View Journal | View Issue

Cite this: *Nanoscale*, 2014, **6**, 11828

A roll-to-roll welding process for planarized silver nanowire electrodes†

Seong Jun Lee,[a] Young-Hoon Kim,[b] Jung Kyu Kim,[ad] Hionsuck Baik,[c] Jae Hoon Park,[a] Jaeki Lee,[d] Jaewook Nam,[d] Jong Hyeok Park,[ad] Tae-Woo Lee,[b] Gi-Ra Yi*[d] and Jeong Ho Cho*[ad]

Received 7th July 2014
Accepted 4th August 2014

DOI: 10.1039/c4nr03771e

www.rsc.org/nanoscale

We demonstrate continuous roll-to-roll production of highly conductive silver network films on a plastic substrate *via* mechanical and chemical welding processes. This process included three essential steps: (i) solvent spraying, (ii) roll compression, and (iii) salt treatment and washing. The sheet resistance of the resulting AgNW film was 5 Ω sq^{-1} at 92% transmittance, which was the lowest sheet resistance and the highest transparency among the values reported previously for solution-processed AgNW electrodes. Moreover, the strong contacts among the AgNWs dramatically enhanced the mechanical stability of the network film. The resulting AgNW film was successfully applied to various organic electronic devices, such as organic field-effect transistors (OFETs), organic light-emitting diodes (OLEDs), and organic solar cells (OSCs).

1. Introduction

Highly conductive silver nanowires (AgNWs) dispersed in a solvent were found to readily form a percolating network at low concentrations during a thin film coating process.[1–5] The percolating AgNW networks enable new applications, and the implementation of the AgNW networks in a variety of devices, including chemical or biological sensors, stretchable conductors, transparent conductive films, and plasmonic waveguides, is expected to improve the device performances significantly. AgNW networks have been extensively explored as an alternative to indium tin oxide (ITO) transparent electrodes for LC displays, touch screens, flexible displays, or solar cells because of their low fabrication costs, high conductivity, transparency, and flexibility.[6–10] Typically, bar-coating processes have been used to produce transparent conductive AgNW films.[2] Thin AgNW (<100 nm in diameter) films offer a sheet resistance of 20 Ω sq^{-1} with 80% transmittance. The sheet resistance may be further enhanced using welding processes involving thermal,[6,9,11] mechanical,[2,11,12] and electrochemical treatments,[2] or integration with other materials.[13,14] Recently, Garnett *et al.* reported that AgNWs could be welded using light-induced local heating around a junction over 1 minute.[15] The surface resistance reached 10 Ω sq^{-1} with 80% transmittance. The preparation of planarized films with ohmic contact between the nanowires poses several challenges but remains critical to the development of thin film electronic devices with high performances and good portability. Their high surface roughness can create electrical shorts across the semiconductor films because some rigid nanowires can pile up and/or protrude to form large local height spikes. Furthermore, low-cost continuous fabrication processes are crucial for commercialization and the achievement of reliable performances.

Here, we demonstrate the continuous roll-to-roll production of highly conductive silver network films on a plastic substrate *via* mechanical and chemical welding processes. The resulting surface resistance was 5 Ω sq^{-1} and yielded a high transmittance (~92%). Three essential steps were undertaken: (i) solvent spraying, (ii) roll compression, and (iii) salt-treatment and washing. These steps minimized the silver network film sheet resistance. A residual poly(vinyl pyrrolidone) (PVP) layer, which had been applied during the AgNW synthesis, was effectively removed by spraying water. A subsequent roll compression process facilitated the formation of electrical connections among the NWs in the network structure. A final salt treatment process increased the strength of the contacts among AgNWs, thereby dramatically enhancing the mechanical stability relative to the stability of the pristine networks. Compared with other welding techniques such as high-intensity pulsed light (HIPL) and laser, our chemical welding process does not require additional external energy and salt solution can be reused.[15,16] The resulting AgNW film was successfully used in organic electronic devices, such as organic field-effect

[a]*SKKU Advanced Institute of Nanotechnology (SAINT), Sungkyunkwan University, Suwon 440-746, Republic of Korea. E-mail: jhcho94@skku.edu*

[b]*Department of Materials Science and Engineering, Pohang University of Science and Technology (POSTECH), Pohang790-784, Republic of Korea*

[c]*Korea Basic Science Institute, Seoul 136-713, Republic of Korea*

[d]*School of Chemical Engineering, Sungkyunkwan University, Suwon 440-746, Republic of Korea. E-mail: yigira@skku.edu*

† Electronic supplementary information (ESI) available. See DOI: 10.1039/c4nr03771e

transistors (OFETs), organic light-emitting diodes (OLEDs), and organic solar cells (OSCs).

2. Experimental section

Roll-to-roll welding of the AgNW film

A 0.5 wt% silver nanowire (AgNW) solution suspended in isopropyl alcohol was purchased from Aldrich Chemical Co. The diameter and length of AgNWs were 115 nm and 20–50 μm, respectively. AgNW solution was coated onto a polyethylene terephthalate (PET) or polyethylene naphthalate (PEN) substrate using the Meyer rod coating method (#14, RD Specialist Inc.). The AgNW film was transferred to the solvent spray system in the first step (Step I). Various solvents (distilled water, methylene chloride (MC), and tetrahydrofuran (THF)) were sprayed at a 0.17 mL s^{-1} flow rate onto the Meyer rod-coated AgNW film, which was subsequently allowed to dry. Secondly, the AgNW film was moved between two compression rollers for a lamination process (Step II). The number of supporting PET films (thickness = 190 μm) was varied to systematically modulate the pressure applied to the AgNW film. Finally, the AgNW film was immersed in salt solutions, such as NaCl and $FeCl_2$ (1, 3, 6, and 10 wt%) for various dipping times (10, 20, 30, 40, 50, and 60 s) and washed in distilled water (Step III). The electrostatic calculation was conducted using OpenFOAM to investigate the potential profile near the AgNW junction (http://www.openfoam.com/, "Official Website of OpenFOAM"). The transmittance of the AgNW films was characterized using a UV-visible spectrophotometer (Agilent 8453) and the sheet resistance was measured according to the four-point probe technique using a Keithley 2182A and 6221.

OFET fabrication

A PEN film coated with indium tin oxide (Peccell Technologies, Inc.) was used as a plastic substrate onto which was fabricated bottom-contact, bottom-gate pentacene and PTCDI-C8 FETs. The ITO surface was then cleaned by UV–ozone treatment (254 nm, 28 mW cm^{-2}) for 30 min. A dimethylformamide solution comprising 10 wt% poly-4-vinylphenol (PVP, M_w = 20 000 g mol^{-1}) and 5 wt% poly(melamine-*co*-formaldehyde) (PMF, M_w = 511 g mol^{-1}) were spin-coated onto the ITO/PEN substrate, followed by thermal annealing for 12 h at 80 °C in a vacuum oven. The specific capacitance of the cross-linked PVP (cPVP) gate dielectric (thickness = 503 nm) was 7.1 nF cm^{-2}. The AgNW source–drain electrodes were patterned onto the cPVP layer through a shadow mask using the spray-coating method. The subsequent three steps (solvent spraying, roll compression, and salt treatment and washing) were applied to decrease the sheet resistance of the AgNW film. The channel length and width were 100 and 1000 μm, respectively. Finally, 50 nm thick pentacene and PTCDI-C8 (Aldrich Chemical Co., no purification) films were deposited from a quartz crucible onto the channel region at a rate of 0.2 Å s^{-1} using an organic molecular beam deposition (OMBD) system. The electrical characteristics of the OFETs were measured at room temperature under ambient conditions in a dark environment using Keithley 2400 equipment and 236 source/measurement units.

OLED fabrication

Onto the prepared AgNW electrode/PEN substrate, a 22 nm thick ZnO layer was deposited by sputtering. After UV-ozone treatment (254 nm, 28 mW cm^{-2}) of the AgNW film for 10 min, 10 nm thick polyethyleneimine (PEI, Sigma-Aldrich) was formed by spin coating. The substrate was then moved into a N_2 glove box, and then Super Yellow (Merck OLED Materials. GmbH, catalog number PDY-132) dissolved in toluene (0.9 wt%) was spin-cast onto the PEI layer (thickness of Super Yellow ~ 230 nm). The structure was then baked at 80 °C for 20 min. The specimen was then transferred into a high-vacuum chamber (<10^{-7} Torr). Finally, 5 nm thick MoO_3 (powder, 99.99%, Sigma-Aldrich) and 80 nm thick Ag (80 nm) were deposited by thermal evaporation. The current–voltage–luminance characteristics were measured using a Keithley 236 source measurement unit and a Minolta CS2000 Spectroradiometer.

OSC fabrication

A 200 nm thick PEDOT:PSS (AI4083, Ossila Ltd) hole conducting layer was coated onto the UV-ozone treated AgNW substrate. The samples were then baked at 115 °C for 15 min on a hotplate. A 3 wt% diiodooctane-containing chlorobenzene solution containing poly({4,8-bis[(2-ethylhexyl)oxy]benzo[1,2*b*:4,5-*b*′]dithiophene-2,6-diyl}{3-fluoro-2-[(2-ethylhexyl)carbonyl]thieno[3,4*b*]-thiophenediyl}) (PTB7) and [6,6]-phenyl C_{71} butyric acid methyl ester ($PC_{71}BM$) in a 1 : 1.5 weight ratio was spin-cast onto the PEDOT:PSS layer to form an 80 nm thick active layer. Prior to depositing a 100 nm thick Al cathode using thermal evaporation under 10^{-7} Torr, a TiO_x layer (6 nm) was coated onto the active layer. The *J*–*V* performances of the OSCs were measured using an Oriel 91193 (a solar simulator with a 1 kW lamp, 100 mW cm^{-2}) using an NREL-calibrated Si solar cell and Keithley 2400 source meters. The cell area was determined using an aperture of 11.43 mm^2. The IPCE measurements were obtained using a Solar Cell QE/IPCE measurement (Zolix Solar Cell Scan 100).

3. Results and discussion

The three essential steps shown in Fig. 1a were integrated into a continuous process that was compatible with the cost- and time-efficient roll-to-roll production method. During the solvent spray step, the AgNW film deposited onto a PET substrate *via* the Meyer rod coating method was washed by spraying a solvent that dissolved the residual polymer layer coating on the NW surfaces. In a subsequent step, the solvent-sprayed AgNW film was mechanically compressed by passing the film between two pressing rollers under different pressures. Finally, the AgNW film was immersed in a salt solution to ionize and re-deposit the Ag atoms, followed by washing with distilled water. Fig. 1b shows optical images and a scanning electron microscopy (SEM) image of the flexible and transparent AgNW films produced by the roll-to-roll process. The optical transmittance (see the inset of Fig. 1b) and the sheet resistance of the resulting

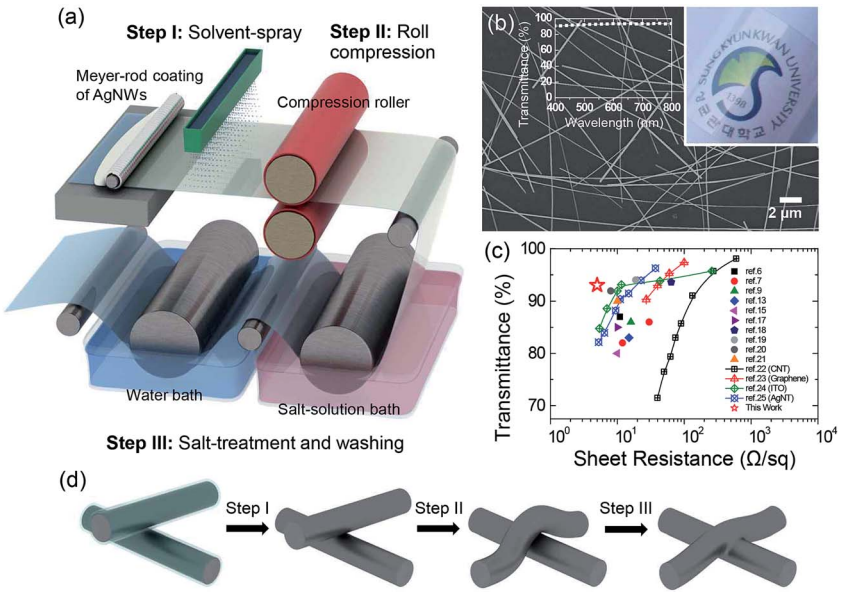

Fig. 1 (a) Schematic diagram showing the steps applied to the AgNW films in this study. The process included (i) solvent spraying, (ii) roll compression, and (iii) salt treatment and washing. (b) Scanning probe microscopy image of the resulting AgNW films. The inset shows the optical transmittance as a function of the wavelength, as well as an optical image of the AgNW films. (c) Comparison of the sheet resistance values measured from this research study, and the transmittance plots collected from other references. (d) Schematic diagram showing the change in the AgNW junction properties during the three steps.

AgNW film were found to be 92% at 550 nm and 5 Ω sq^{-1}, respectively. To the best of our knowledge, this is the highest transparency and lowest resistivity among the values reported previously for solution-processed AgNW electrodes (Fig. 1c).[6,7,9,13,15,17–25] Fig. 1d shows that the AgNW junction properties changed over the course of the three steps, as discussed below.

As indicated in "Step I" of Fig. 1a, water was sprayed onto the film to remove any residual poly(vinyl pyrrolidone) (PVP) surfactant, which had coated the wires through weak non-covalent bonding or van der Waals forces.[26] Methylene chloride (MC) and tetrahydrofuran (THF) were also sprayed onto the film to wash away PVP. The marginal solvent, MC, and a good solvent, water, dramatically reduced the sheet resistance from 56 Ω sq^{-1} to 37 Ω sq^{-1} for MC and to 26 Ω sq^{-1} for water after a 2 min spray washing period. THF treatment, however, did not significantly change the resistance because THF was a non-solvent for PVP. The TEM images of the pristine and water-sprayed AgNWs are shown in the right panel of Fig. 2a. A residual PVP layer with several tens of nanometers thickness was effectively removed by spraying water, which facilitated the electrical connections among the NWs in the network structure and dramatically reduced the sheet resistance ("Step I" in Fig. 1d). The removal of the residual PVP layer during water spraying was confirmed using energy-dispersive X-ray (EDX) measurements, which showed that the C-to-Ag atomic ratio was dramatically reduced from 0.15 to 0.06 (Fig. S1†). Note that during the solvent spray process, the optical transmittance at 550 nm remained at 92%.

In the second step, the roll compression process was applied to the solvent-sprayed AgNWs (Fig. 1a). Supporting PET films were added between the compression roll and the sample to systematically increase the pressure applied to the AgNW film. All samples exhibited a gradual decrease and saturation of the sheet resistance as the number of the supporting films was increased (Fig. 2b). The R/R_0 (R_0 is the sheet resistance of the AgNW films without roll compression) value is shown in the inset of Fig. 2b. The pristine and THF-sprayed AgNW films displayed only a 30% reduction in the sheet resistance. The MC- and distilled water-sprayed AgNW films, on the other hand, displayed a significant decrease in the sheet resistance, even under the same compression pressure, due to the reduced residual PVP layers present on the AgNW surfaces. The water-spayed AgNW film, which was compressed using 7 supporting PET films, yielded a sheet resistance of 10 Ω sq^{-1}. The right panel of Fig. 2b shows scanning electron microscopy (SEM) images of the tilted views of the water-sprayed AgNW films before and after roll compression. The water-sprayed AgNWs piled up on the other AgNWs, which exhibited structures similar to that of the Meyer-rod coated pristine AgNWs. After lamination, the junctions among the NWs became partially compressed, which broadened the surface contact area at the junctions ("Step II" in Fig. 1d).

In the final step, immersion in a salt solution and subsequent washing further decreased the sheet resistance of the AgNW film (Fig. 1a). The water-sprayed and compressed AgNW film with a sheet resistance of 10 Ω sq^{-1} was immersed in a NaCl solution having different concentrations (1, 3, 6, and 10 wt%). Fig. 2c shows the change in the sheet resistance of the AgNW film as a function of the dipping time in the NaCl solution. The sheet resistance dramatically decreased with increasing immersion time and a higher NaCl concentration yielded a more dramatic decrease in the sheet resistance.

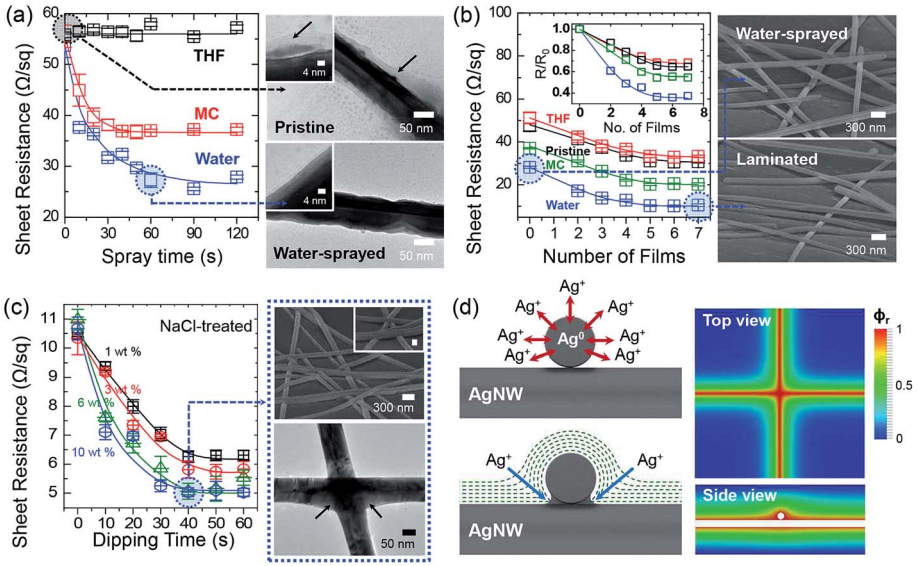

Fig. 2 (a) Sheet resistance *vs.* the spray time for various solvents, including water, MC, and THF. The right panel shows TEM images of the pristine AgNWs and the water-sprayed AgNWs. The arrow indicates the residual PVP layer. (b) Changes in the AgNW film sheet resistance as a function of the number of supporting PET films applied during the roll compression process. The right panel shows SEM images before and after roll compression. (c) Changes in the AgNW film sheet resistance as a function of the dipping time in a NaCl solution (1, 3, 6, and 10 wt% NaCl in water). The top right panel shows SEM images of the NaCl-treated AgNWs (40 s). The scale bar of the enlarged figure in the inset indicates 100 nm. The right lower panel shows a TEM image of the NaCl-treated AgNWs (40 s). The arrows indicate fusion at the junctions between AgNWs. (d) AgNW welding mechanism during the NaCl treatment. Ag atoms were ionized making AgNWs negatively charged. In the electrostatic calculation, potential near the junction across AgNWs are higher than other areas, which may cause the relatively higher deposition of Ag. Red and blue colors indicate the maximum and minimum value of reduced potential ($\phi_r = \phi/\phi_{surface}$) normalized with surface potential, respectively.

As discussed in previous studies of the dissolution of silver nanoparticles,[27–30] in the presence of chloride ions (Cl^-) and dissolved oxygen in water, silver atoms in AgNWs may be dissolved slowly to produce solvated silver ions (Ag^+) due to redox reactions. Alternatively, silver ions adsorbed onto the NW surfaces may dissolve. The dissolution of Ag^+ ions was confirmed by analyzing the NaCl solution using ICP-MS after incubating the AgNW film in NaCl solution. Ag^+ was detected at 1.9 ppb after a 20 s incubation period or at 10.5 ppb after a 60 s incubation period. Molecular oxygen adsorbed onto the silver surfaces and dissociated to form atomic oxygen between 200 K and 500 K; therefore, atomic oxygen on the silver surfaces could potentially block the re-deposition of Ag^+ onto the AgNW surfaces. There is a good chance that a small quantity of Ag^+ ions could be re-deposited onto the relatively more active AgNW surface because the oxygen concentration in water was quite limited and the adsorption process was dynamically equilibrated. The re-deposition of Ag^+ ions onto both the surfaces and junctions of the AgNWs led to strong fusion among the AgNWs, as shown in the right panel of Fig. 2c and in "Step III" in Fig. 1d. We speculated that the nanowires could become negatively charged upon ionization of silver, thereby generating a uniform electrostatic potential field around the nanowire [$V(r) \sim \ln(1/r)$] (ref. 31) and a non-uniform potential field near the junction, as illustrated in Fig. 2d. In the electrostatic calculation using OpenFOAM, the potential near the junction across AgNWs is higher than other areas. Therefore, the re-deposition of Ag^+ ions near the junction was preferred over other areas, which may have enhanced the conductivity after the salt treatment. The TEM images shown in Fig. 2c indicate that Ag^+ ions could be deposited more commonly at the junctions that formed a bridge. This mechanism may be ascribed to Ostwald ripening because the Laplace pressure at the junction was lower than on the plain surfaces of the AgNWs. Another $FeCl_2$ salt was also applied to the AgNWs in an effort to provide similar behaviors to those observed in the case of NaCl (Fig. S2†). The minimum sheet resistance of the AgNW films was found to be 5 Ω sq^{-1} and the optical transmittance was 92% at 550 nm. The haze (total diffusion/total transmittance) at 550 nm was 7.26%. Importantly, the root-mean-square (rms) roughness decreased dramatically after the three steps from 68.1 nm to 45.8 nm (Fig. S3†).

The mechanical flexibility and robustness of the AgNW films were investigated by measuring the sheet resistance under a compression or tension of at most 2% strain (Fig. 3a).[32,33] The pristine AgNW film exhibited a dramatic increase in the sheet resistance at a 2% strain; however, the NaCl-treated film yielded much higher stability due to the strong fusion properties of the NWs. Fatigue tests were performed on the AgNW films. The sheet resistance of the NaCl-treated AgNW films remained constant, even after 400 cycles of 1% bending along the longitudinal direction (Fig. 3b). The AgNWs were transferred onto a newspaper to test their mechanical properties under extreme conditions, as shown in the inset of Fig. 3b. After crushing and then unfolding the film on a newspaper, the AgNW film remained conductive, with only a limited change in the resistance, from 15 to 37 Ω sq^{-1}.[25]

Ultra-transparent and ultra-conductive AgNWs were successfully used in flexible transparent organic electronic

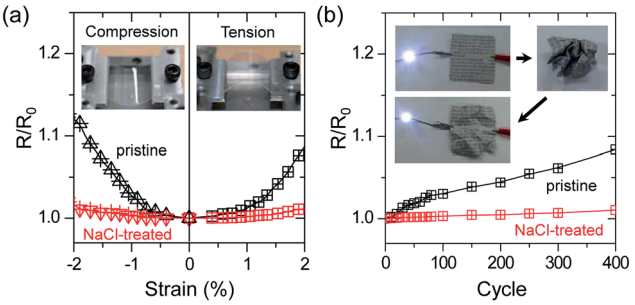

Fig. 3 (a) R/R_0 as a function of the strain level (±2%). (b) R/R_0 as a function of the cycling number during a 1% strain tension. The inset shows photographs of the AgNW film coated onto a newspaper. After crushing and unfolding, the paper remained conducting (the resistance increased from 15 to 37 Ω sq^{-1}).

devices, such as organic field-effect transistors (OFETs), organic light-emitting diodes (OLEDs), and organic solar cells (OSCs).

Transparent flexible OFETs prepared using our optimized AgNW source–drain electrodes were fabricated, as shown in the inset of Fig. 4a. ITO and cross-linked poly-4-vinylphenol (cPVP) were used as the gate electrode and gate dielectric, respectively. Source–drain electrodes were prepared by spray-coating an AgNW dispersion onto the cPVP surface through a shadow mask, followed by water spraying, roll compression, and NaCl treatment/washing. Both p-type pentacene and n-type PTCDI-C8 were thermally deposited onto the channel regions. Fig. 4a shows the optical transmittance of an OFET array fabricated on a polyethylene naphthalate (PEN) substrate over the visible and near-infrared spectral range. The average transparency of a neat PEN film was approximately 88% in the range 400–1000 nm. The overall average transparency of a film after depositing an OFET array onto the PEN substrate decreased slightly to around 83%. Fig. 4b and c show typical output and transfer characteristics of the resulting devices, respectively. Both p-type and n-type devices exhibited reasonable gate modulation of I_D in both the linear and saturation regimes (Fig. 4b). Although the AgNW source–drain electrode surfaces were extremely rough compared to the surfaces of the thermally evaporated Au, our AgNW electrodes provided good device performances from both pentacene and PTCDI-C8 FETs (Fig. 4c). For example, the p-type pentacene OFETs exhibited an extracted hole mobility of 0.06 ± 0.02 $cm^2\ V^{-1}\ s^{-1}$ with an on/off current ratio of ~10^5, whereas the n-type PTCDI-C8 OFETs exhibited an electron mobility of 0.04 ± 0.02 $cm^2\ V^{-1}\ s^{-1}$ with an on/off current ratio of ~10^5 (using $L = 100$ μm and $W = 1000$ μm for calculation). These hole and electron mobility values were comparable to those of OFETs prepared using thermally evaporated metal source–drain bottom contacts, $\mu_h = 0.08\ cm^2\ V^{-1}\ s^{-1}$, for a pentacene OFET with Au contacts, or $\mu_e = 0.05\ cm^2\ V^{-1}\ s^{-1}$ for a PTCDI-C8 OFET with Au contacts.[34] While the as-calculated mobilities are overestimated values considering the spiked edges of the AgNW electrodes (L must be shorter and W must be larger effectively), it should be noted that electrodes with a larger effective W–L ratio are beneficial for generating a higher current level than those made in the pad-type.

The transparent and flexible AgNWs were next used in inverted OLEDs, as shown in Fig. 4d. The basic architecture of our OLED consisted of five layers: an electron injecting ZnO, an electron injecting polyethyleneimine (PEI) interlayer,[35] an emitting Super Yellow layer, a hole injecting MoO_3 layer, and a Ag anode layer. Fig. 4e shows the current density–voltage–luminance characteristics of OLEDs prepared with an AgNW cathode. These properties were compared with those of a reference OLED prepared with ITO. The devices prepared with AgNWs showed a relatively higher current density and luminance compared to the ITO. The lower resistance of the AgNWs (5 Ω sq^{-1}) and the small electron injection energy barrier from the AgNWs (work function ~ 4.2 eV) to ZnO (lowest unoccupied molecular orbital (LUMO) energy level of 4.4 eV) increased the electron injection and current density, and also its higher transmittance of the AgNWs (92% at 550 nm) increased the luminance.[36–38] Our OLED prepared with AgNWs convincingly displayed a higher current density and luminance compared to the ITO-based OLED at any given applied voltage. The higher leakage current, resulting from the high roughness, produced a slightly lower luminous efficiency at a low voltage of <4 V. The luminous current and power efficiencies at high voltages, >4 V, were comparable (9.61 cd A^{-1} and 4.31 lm W^{-1} at 100 cd m^{-2}, 12.02 cd A^{-1} and 3.77 lm W^{-1} at 1000 cd m^{-2}) to the corresponding values obtained from devices prepared with ITO (9.55 cd A^{-1} and 4.28 lm W^{-1} at 100 cd m^{-2}, 13.02 cd A^{-1} and 3.72 lm W^{-1} at 1000 cd m^{-2}), as shown in Fig. 4f. Therefore, our AgNWs offered a good strategy for preparing flexible displays and lighting applications because the AgNWs could replace the brittle ITO electrodes while providing comparable luminous efficiencies.

Finally, the transparent flexible AgNWs were used in OSCs, as shown in Fig. 4g. The basic architecture of our OSCs included four layers: a hole-injecting poly(3,4-ethylenedioxythiophene):poly(styrene sulfonic acid) (PEDOT:PSS) layer, a bulk heterojunction PTB7/$PC_{71}BM$ layer, an electron injecting TiO_x layer, and an Al cathode layer. Fig. 4h shows the photocurrent density–voltage characteristics of the OSCs prepared using the AgNWs as the anodes. The values were compared with those obtained from a reference OSC prepared with ITO. The OSCs prepared with the AgNW anodes provided an open-circuit voltage (V_{oc}), a short-circuit current (J_{sc}), and a fill factor (FF) of 0.72 V, 12.7 mA cm^{-2}, and 48.9%, respectively (V_{oc}: 0.67 V, J_{sc}: 14.4 mA cm^{-2}, and FF: 48.0% for the ITO device). The resulting AgNW device exhibited a power conversion efficiency (PCE) of 4.47%, which was comparable to the value obtained from an ITO-based device (4.62%), despite the high roughness and low work function of the AgNW film. This excellent performance presumably arose from the low resistance and high transmittance of the AgNW film compared to the ITO film, which compensated for the roughness and work function effects.[39] The incident photon to electron conversion efficiency (IPCE) spectra of the devices were recorded and are plotted in Fig. 3i. The AgNW films prepared here were successfully used as solution-processable anodes in flexible OSCs. Overall, the three basic building units of organic electronic devices including OFETs, OLEDs, and OSCs based on the

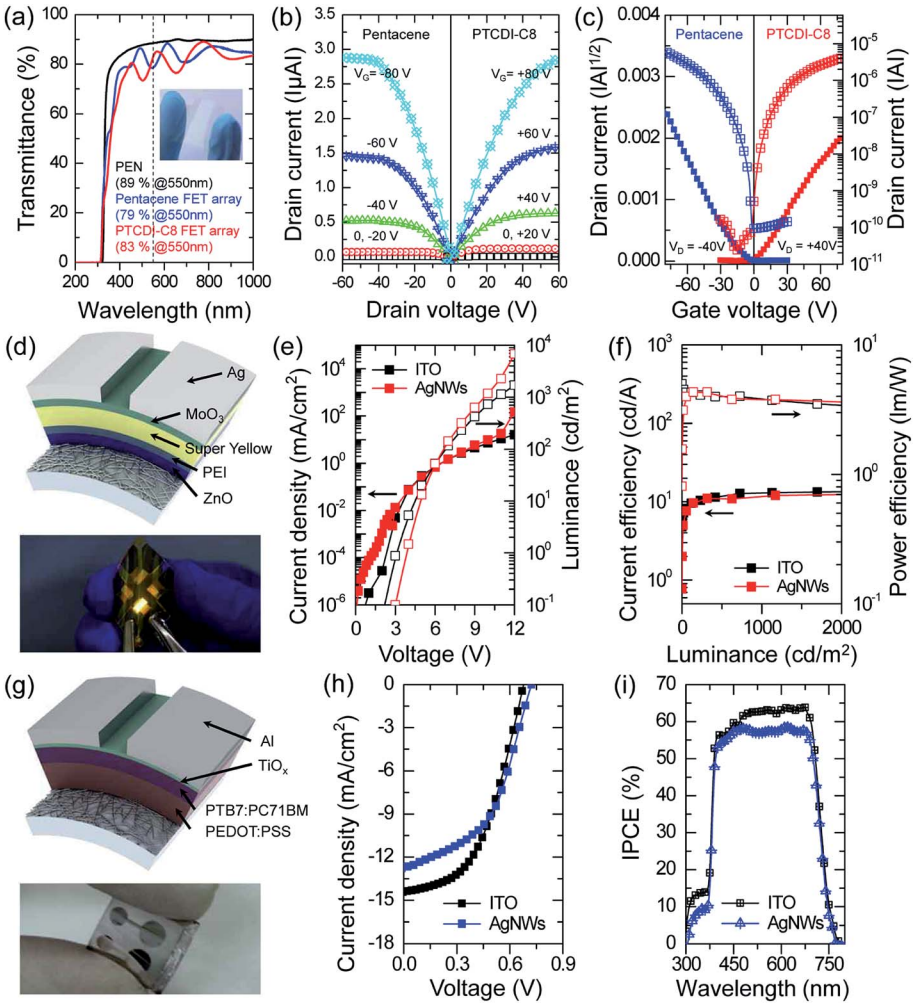

Fig. 4 (a) UV-vis spectra of a PEN substrate with a pentacene or PTCDI-C8 FET array formed by AgNW source–drain electrodes. The inset shows a photograph of the pentacene FET array on a PEN substrate. (b) Transfer and (c) output characteristics of the resulting transparent and flexible p-type pentacene and n-type PTCDI-C8 FETs. (d) Schematic diagram of an inverted PLED based on an AgNW cathode. The lower panel shows a light-emission image under bending. (e) Current density–voltage luminance characteristics of PLEDs prepared using ITO or AgNW cathodes. (f) Current efficiency and power efficiency as a function of the luminance of the PLEDs prepared using ITO or AgNW cathodes. (g) Schematic diagram and a photographic image of an OSC based on the AgNW anode. (h) Photocurrent–voltage (J–V) and (i) IPCE wavelength characteristics of OSCs prepared using ITO or AgNW anodes.

AgNW electrodes exhibited comparable device performances with those made of conventional but brittle Au or ITO electrodes.

4. Conclusions

In conclusion, the continuous roll-to-roll production of highly conductive AgNW films on plastic substrates, including the application of mechanical and chemical welding processes, was demonstrated. This process included three essential steps: (i) solvent spraying, (ii) roll compression, and (iii) salt treatment and washing. The sheet resistance of the resulting AgNW film decreased dramatically to 5 Ω sq^{-1} at a 92% of transmittance. The strong contacts among the AgNWs, which formed after the three steps, dramatically enhanced the mechanical stability of the network film. The resulting AgNW film was successfully used various organic electronic applications, such as OFETs, OLEDs, and OSCs.

Acknowledgements

This work was supported by the KANEKA/SKKU Incubation Center (financially supported by Kaneka Corp. in Japan), a grant from the Center for Advanced Soft Electronics (CASE) under the Global Frontier Research Program (2013M3A6A5073177) and the Basic Science Research Program (2009-0083540, 2014M3A9B8023471, and 2010-0029409) of the National Research Foundation of Korea (NRF) funded by the Ministry of Education, Science and Technology, Korea. We appreciate Prof. Dov Levine (Technion) about the helpful discussion on the welding mechanism of AgNWs.

References

1 M. K. Song, D. S. You, K. A. Lim, S. J. Park, S. H. Jung, C. S. Kim, D. H. Kim, D. G. Kim, J. K. Kim, J. Y. Park, Y. C. Kang, J. H. Heo, S. H. Jin, J. H. Park and J. W. Kang, *Adv. Funct. Mater.*, 2013, **23**, 4177–4184.
2 L. Hu, H. S. Kim, J. Y. Lee, P. Peumans and Y. Cui, *ACS Nano*, 2010, **4**, 2955–2963.
3 V. Scardaci, R. Coull, P. E. Lyons, D. Rickard and J. N. Coleman, *Small*, 2011, **7**, 2621–2628.
4 J. H. Lee, P. Lee, H. Lee, D. Lee, S. S. Lee and S. H. Ko, *Nanoscale*, 2012, **4**, 6408–6414.
5 J. H. Lee, P. Lee, D. Lee, S. S. Lee and S. H. Ko, *Cryst. Growth Des.*, 2012, **12**, 5598–5605.
6 D. S. Leem, A. Edwards, M. Faist, J. Nelson, D. D. Bradley and J. C. de Mello, *Adv. Mater.*, 2011, **23**, 4371–4375.
7 Z. Yu, Q. Zhang, L. Li, Q. Chen, X. Niu, J. Liu and Q. Pei, *Adv. Mater.*, 2011, **23**, 664–668.
8 A. Tao, F. Kim, C. Hess, J. Goldberger, R. He, Y. Sun, Y. Xia and P. Yang, *Nano Lett.*, 2003, **3**, 1229–1233.
9 J. Y. Lee, S. T. Connor, Y. Cui and P. Peumans, *Nano Lett.*, 2008, **8**, 689–692.
10 P. Lee, J. Lee, H. Lee, J. Yeo, S. Hong, K. H. Nam, D. Lee, S. S. Lee and S. H. Ko, *Adv. Mater.*, 2012, **24**, 3326–3332.
11 L. Yang, T. Zhang, H. Zhou, S. C. Price, B. J. Wiley and W. You, *ACS Appl. Mater. Interfaces*, 2011, **3**, 4075–4084.
12 W. Gaynor, G. F. Burkhard, M. D. McGehee and P. Peumans, *Adv. Mater.*, 2011, **23**, 2905–2910.
13 R. Zhu, C. H. Chung, K. C. Cha, W. Yang, Y. B. Zheng, H. Zhou, T. B. Song, C. C. Chen, P. S. Weiss, G. Li and Y. Yang, *ACS Nano*, 2011, **5**, 9877–9882.
14 J. Lee, P. Lee, H. B. Lee, S. Hong, I. Lee, J. Yeo, S. S. Lee, T. S. Kim, D. Lee and S. H. Ko, *Adv. Funct. Mater.*, 2013, **23**, 4171–4176.
15 E. C. Garnett, W. Cai, J. J. Cha, F. Mahmood, S. T. Connor, M. G. Christoforo, Y. Cui, M. D. McGehee and M. L. Brongersma, *Nat. Mater.*, 2012, **11**, 241–249.
16 J. Jiu, M. Nogi, T. Sugahara, T. Tokuno, T. Araki, N. Komoda, K. Suganuma, H. Uchida and K. Shinozaki, *J. Mater. Chem.*, 2012, **22**, 23561–23567.
17 A. R. Madaria, A. Kumar, F. N. Ishikawa and C. Zhou, *Nano Res.*, 2010, **3**, 564–573.
18 I. N. Kholmanov, C. W. Magnuson, A. E. Aliev, H. Li, B. Zhang, J. W. Suk, L. L. Zhang, E. Peng, S. H. Mousavi, A. B. Khanikaev, R. Piner, G. Shvets and R. s. Ruoff, *Nano Lett.*, 2012, **12**, 5679–5683.
19 J. M. Lee, I. H. Lee, T. S. Kim and J. Y. Lee, *Small*, 2013, **9**, 2887–2894.
20 A. R. Kim, Y. L. Won, K. H. Woo, C. H. Kim and J. H. Moon, *ACS Nano*, 2013, **7**, 1081–1091.
21 T. Kim, Y. W. Kim, H. S. Lee, H. Kim, W. S. Yang and K. S. Suh, *Adv. Funct. Mater.*, 2013, **23**, 1250–1255.
22 H. Z. Geng, K. K. Kim, K. P. So, Y. S. Lee, Y. K. Chang and Y. H. Lee, *J. Am. Chem. Soc.*, 2007, **129**, 7758–7759.
23 S. Bae, H. Kim, Y. Lee, X. Xu, J.-S. Park, Y. Zheng, J. Balakrishnan, T. Lei, H. R. Kim, Y. I. Song, Y.-J. Kim, K. S. Kim, B. Ozyilmaz, J.-H. Ahn, B. H. Hong and S. Lijima, *Nat. Nanotechnol.*, 2010, **5**, 574–578.
24 A. Schindler, J. Brill, N. Fruehauf, J. P. Novak and Z. Yaniv, *Physica E Low Dimens Syst Nanostruct*, 2007, **37**, 119–123.
25 H. Wu, D. Kong, Z. Ruan, P. C. Hsu, S. Wang, Z. Yu, T. J. Carney, L. Hu, S. Fan and Y. Cui, *Nat. Nanotechnol.*, 2013, **8**, 421–425.
26 P. S. Mdluli, N. M. Sosibo, P. N. Mashazi, T. Nyokong, R. T. Tshikhudo, A. Skepu and E. Van Der Lingen, *J. Mol. Struct.*, 2011, **1004**, 131–137.
27 J. Liu and R. H. Hurt, *Environ. Sci. Technol.*, 2010, **44**, 2169–2175.
28 C. N. Lok, C. M. Ho, R. Chen, Q. Y. He, W. Y. Yu, H. Sun, P. K. H. Tam, J. F. Chiu and C. M. Che, *JBIC, J. Biol. Inorg. Chem.*, 2007, **12**, 527–534.
29 J. Dobias and R. Bernier-Latmani, *Environ. Sci. Technol.*, 2013, **47**, 4140–4146.
30 D. Y. Shin, G. R. Yi, D. Lee, J. Park, Y.-B. Lee, I. Hwang and S. Chun, *Nanoscale*, 2013, **5**, 5043–5052.
31 Z. Popovic and B. D. Popovic, *Introductory Electromagnetics*, Prentice hall, 1999.
32 X. Y. Zeng, Q. K. Zhang, R. M. Yu and C. Z. Lu, *Adv. Mater.*, 2010, **22**, 4484–4488.
33 M. S. Lee, K. S. Lee, S. Y. Kim, H. J. Lee, J. H. Park, K. H. Choi, H. K. Kim, D. G. Kim, D. Y. Lee and S. W. Nam, *Nano Lett.*, 2013, **13**, 2814–2821.
34 J. S. Lee, N. H. Kim, M. S. Kang, H. Yu, D. R. Lee, J. H. Oh, S. T. Chang and J. H. Cho, *Small*, 2013, **9**, 2817–2825.
35 Y. Zhou, C. Fuentes Hernandez, J. Shim, J. Meyer, A. J. Giordano, H. Li, P. Winget, T. Papadopoulos, H. Cheun and J. Kim, *Science*, 2012, **336**, 327–332.
36 D. Kabra, L. P. Lu, M. H. Song, H. J. Snaith and R. H. Friend, *Adv. Mater.*, 2010, **22**, 3194–3198.
37 T. W. Lee, J. Hwang and S. Y. Min, *ChemSusChem*, 2010, **3**, 1021–1023.
38 B. R. Lee, H. Choi, J. S. Park, H. J. Lee, S. O. Kim, J. Y. Kim and M. H. Song, *J. Mater. Chem.*, 2011, **21**, 2051–2053.
39 D. H. Wang, A. K. K. Kyaw, V. Gupta, G. C. Bazan and A. J. Heeger, *Adv. Energy Mater.*, 2013, **3**, 1161–1165.